





## Article

# A Composite Exponential Reaching Law Based SMC with Rotating Sliding Surface Selection Mechanism for Two Level Three Phase VSI in Vehicle to Load Applications

Faheem Haroon<sup>1</sup>, Muhammad Aamir<sup>2</sup>, Assad Waqar<sup>1,\*</sup>, Saeed Mian Qaisar<sup>3,4,\*</sup>, Syed Umaid Ali<sup>1</sup>  
and Abdulaziz Turki Almaktoom<sup>5,\*</sup>

<sup>1</sup> Department of Electrical Engineering, Bahria School of Engineering and Applied Sciences Islamabad Campus (BSEAS-IC), Islamabad 44000, Pakistan

<sup>2</sup> Pak-Austria Fachhochschule Institute of Applied Sciences and Technology, Haripur 22620, Pakistan

<sup>3</sup> Electrical and Computer Engineering Department, Effat University, Jeddah 22332, Saudi Arabia

<sup>4</sup> Communication and Signal Processing Lab, Energy and Technology Research Center, Effat University, Jeddah 22332, Saudi Arabia

<sup>5</sup> Supply Chain Management Department, Effat University, Jeddah 22332, Saudi Arabia

\* Correspondence: asadwaqar.buic@bahria.edu.pk (A.W.); sqaisar@effatuniversity.edu.sa (S.M.Q.); abalmaktoom@effatuniversity.edu.sa (A.T.A.)

**Abstract:** Voltage source inverters (VSIs) are an integral part of electrical vehicles (EVs) to enhance the reliability of the supply power to critical loads in vehicle to load (V2L) applications. The inherent properties of sliding mode control (SMC) makes it one of the best available options to achieve the desired voltage quality under variable load conditions. The intrinsic characteristic of robustness associated with SMC is generally achieved at the cost of unwanted chattering along the sliding surface. To manage this compromise better, optimal selection of sliding surface coefficient is applied with the proposed composite exponential reaching law (C-ERL). The novelty of the proposed C-ERL is associated with the intelligent mix of the exponential, power, and difference functions blended with the rotating sliding surface selection (RSS) technique for three phase two level VSI. Moreover, the proposed reaching law along with the power rate exponential reaching law (PRERL), enhanced exponential reaching law (EERL), and repetitive reaching law (RRL) were implemented on two level three phase VSI under variable load conditions. A comparative analysis strongly advocates the authenticity and effectiveness of the proposed reaching law in achieving a well-regulated output voltage with a high level of robustness, reduced chattering, and low %THD.

**Keywords:** sliding mode control; three phase voltage source inverter; reaching law; chattering; sliding surface



**Citation:** Haroon, F.; Aamir, M.; Waqar, A.; Mian Qaisar, S.; Ali, S.U.; Almaktoom, A.T. A Composite Exponential Reaching Law Based SMC with Rotating Sliding Surface Selection Mechanism for Two Level Three Phase VSI in Vehicle to Load Applications. *Energies* **2023**, *16*, 346. <https://doi.org/10.3390/en16010346>

Academic Editors: Hervé Morel and Md Rasheduzzaman

Received: 14 November 2022

Revised: 16 December 2022

Accepted: 20 December 2022

Published: 28 December 2022



**Copyright:** © 2022 by the authors. Licensee MDPI, Basel, Switzerland. This article is an open access article distributed under the terms and conditions of the Creative Commons Attribution (CC BY) license (<https://creativecommons.org/licenses/by/4.0/>).

## 1. Introduction

Electrical vehicles (EVs) in the vehicle to load (V2L) mode of operation are considered one of the best ways to enhance the reliability of supply to critical loads such as medical equipment in hospitals, military loads, communication systems, data processing, and storage systems, etc. [1–3]. In the V2L mode of operation, shown in Figure 1, EVs ensure uninterrupted power supply to critical loads in the case of main grid failure and operate in stand-alone mode for the electrification of utilities and expensive loads in remote areas [4–6]. Nowadays, EVs use a more or less similar power electronic interface to derive critical loads in V2L (i.e., three phase two level voltage source inverter (TLVSIs)) [7]. In order to handle sensitivity associated with critical loads, three phase TLVSI must have a high disturbance rejection capacity, exceptional voltage regulation with low total harmonic distortion (%THD), fast transient, and excellent dynamic response under sudden load variations [8].

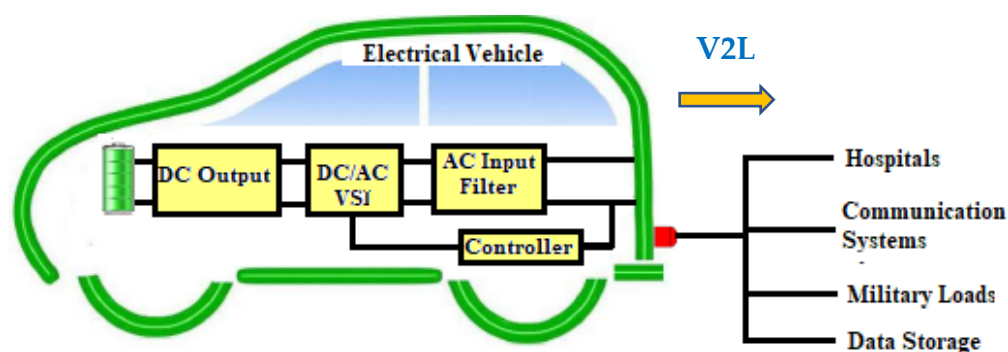


**Figure 1.** Schematic of the V2L operation of the system.

In today's world, operations of systems associated with voltage source inverters (VSIs) are meeting the stability constraints to overcome economic and environmental concerns. Moreover, hybrid energy management systems are seeking effective control mechanisms to handle constraints associated with the load-frequency balance [9]. The intrinsic properties of sliding mode control (SMC) such as high robustness, simple design, and reduced order make it special from other control techniques [10]. Moreover, a VSI with SMC control requires effective and adaptive switching control reaching law and dynamic sliding surface characterization to ensure voltage regulation with the minimum steady state error and reaching time under extreme operating conditions. While achieving these objectives for V2L operation, fast and infinite switching at the inverter takes place. The limitations of switching frequency and current inertia associated with VSI lead to a major problem along the sliding surface, termed as chattering. In order to avoid chattering without compromising much on robustness and dynamic behavior, numerous efforts worth mentioning have been made, mainly focusing on the sliding surface design and reaching law design.

In [11], Gudey and Gupta proposed fast terminal sliding mode control (FTSMC) for VSI. FTSMC is based on the sliding surface using linear and nonlinear characteristics. This nonlinear surface design based FTSMC reduced the tracking and sliding time but missed the luck to reduce the tracking error significantly. Fractional order SMC for a distributed energy resource system with black start functionality was proposed in [12] to ensure a regulated voltage supply under unbalanced load conditions. However, these objectives were achieved at the cost computational burden and complexity in implementation. In [13], it was shown that the fixed value of the sliding surface coefficient is a trade-off between the tracking time under current disturbances and the time consumed by system states to reach the sliding surface. In order to handle this trade-off better, various efforts have been made to design a sliding surface with an adjustable sliding surface coefficient [14,15]. The concept of rotation of the sliding surface technique was proposed in [16], the idea of which was derived from the 1D and 2D fuzzy based rules adopted in [17,18], respectively. Komurkugil et al. [19], motivated by the idea of single input fuzzy logic controller (SIFLC) based on state variables, adjusted the value of the sliding surface coefficient, which led to the rotating sliding surface mechanism, applied and tested on a VSI.

SMC guarantees asymptotic convergence of system states to the sliding surface with convergence time associated with the value of reaching the law control gain [20]. Moreover, the reaching law is beneficial in ensuring the reaching condition along with specifying the dynamic behavior of the motion of state variables in the reaching phase [21]. Many variants of conventional reaching laws were addressed in [20] such as the constant reaching law (C-RL), power rate reaching law (PR-RL), and constant hybrid with proportional reaching law. Thus, to enhance the proficiency of handling the trade-off between convergence time, chattering, and robustness better, exponential reaching law (E-RL) based SMC has been adopted widely in many nonlinear systems [22]. In [23], slight modifications to E-RL proved beneficial in achieving reduced chattering with low total harmonic distortion (%THD). Moreover, the enhanced exponential reaching law (EERL) was proposed in [24] to achieve a fast transient response with reduced chattering. Cos function integrated with

power function was used to modify E-RL in [25,26] to achieve an improved convergence rate with evident chattering reduction along the surface. However, the restricted control gain magnitude limits the reaching time and chattering reduction capacity. The power rate exponential reaching (PRERL) and fractional power rate reaching law (FPRRL) were proposed in [27,28], respectively. Both reaching laws have succeeded in achieving marginal improvement in a reduction to the reaching time, robustness, and chattering. Moreover, in [29], the discrete time repetitive reaching law (RRL) based SMC was proposed for three phase VSI to achieve an improved steady state response with reduced chattering.

Therefore, multiple constraints associated with the already proposed reaching laws, particularly for three phase TLVSI, provides enough motivation to develop a state-of-the-art reaching law that ensures an improved convergence rate, robustness of a system with a reduced level of chattering, and %THD.

A few of the limitations, necessary to cater to, are listed below:

- i. Most of the scholarly work has focused mainly on one of the two key challenges associated with designing SMC based three phase VSI (i.e., effective reaching law and appropriate sliding surface).
- ii. Value of the reaching law gain performs a key role in achieving robustness, where a large value of reaching law gain serves to achieve a higher reaching speed with undesirable chattering along the sliding surface. Similarly, chattering along the surface reduces at a lower value of the reaching law gain but at the cost of the slow reaching speed of system states to the surface. Therefore, this trade-off is critical to handle and extensive high rate scholarly work has so far been conducted, however, it is the call of the day to handle this trade-off in a much better way for sensitive loads.
- iii. Robustness of the three phase VSI is guaranteed when the system states reach the sliding surface, however, the dynamic performance and behavior of the inverter is strictly associated with proper selection of the value of the sliding coefficient. At a smaller value of the sliding coefficient, output voltage of the inverter will take more time to track its reference due to a slower convergence rate along the sliding surface. While at a larger value of the sliding coefficient, the tracking time is reduced with an increase in the reaching time.
- iv. Following the severity of the above-mentioned issues, several effective techniques have so far been proposed. Keeping in mind the sensitivity associated with three phase TLVSI for V2L applications, there is still much room of improvement to achieve a high level of robustness with mitigated chattering.

Targeting the above-mentioned issues, the key contributions of this article are numbered below:

- i. A novel reaching law function to set the value of control gain considering the distance of the system states from the sliding surface for three phase TLVSI was proposed. A higher value of control gain was set at a greater distance to ensure a high robustness and convergence rate, while the value of the control gain was lowered following the decreasing distance, and it vanished on the surface to mitigate chattering.
- ii. A three phase VSI with SMC based control for V2L applications was designed, comprising a rotating sliding surface selection mechanism based on single input fuzzy logic control (SIFLC) and the proposed novel composite reaching law.
- iii. Behavior of the proposed reaching law based SMC along with PRERL [27], RRL [29], and EERL [24] were tested on different values of gain, for the three phase VSI in the  $\alpha\beta$  stationary frame. It was shown from the comparative analysis that the proposed reaching law performed remarkably well in achieving a low reaching time at a low value of gain and chattering as well as an extremely low reaching time without compromising much on chattering at a high value of gain.
- iv. The proposed reaching law based SMC, PRERL [27], RRL [29], and EERL [24] were tested on a three phase TLVSI under extreme conditions of nonlinear load. Results showed that the proposed reaching law has an extremely fast transient response with excellent voltage regulation from no load to full-load conditions. Moreover, with a fast

convergence rate and high degree of robustness, the proposed reaching law offered low %THD and reduced chattering.

### 2. System Description

To derive critical loads in V2L mode, EVs were equipped with three phase TLVSI [7]. The proposed control system design with H-bridge circuit topology for three phase VSI is shown in Figure 2. The filter inductor, capacitor, and inductor’s parasitic resistance is represented as  $L$ ,  $C$ , and  $r$ , respectively. The input DC voltage from the battery of the EV and three phase load connected at output is shown as  $V_S$  and  $Z$ , respectively. Control feedback variables of interest are the voltage across capacitor and current through the filter capacitor, which are shown as  $V_{c(abc)}$  and  $i_{c(abc)}$ , respectively. The control scheme of the proposed law was designed in a stationary  $(\alpha, \beta)$  reference frame.

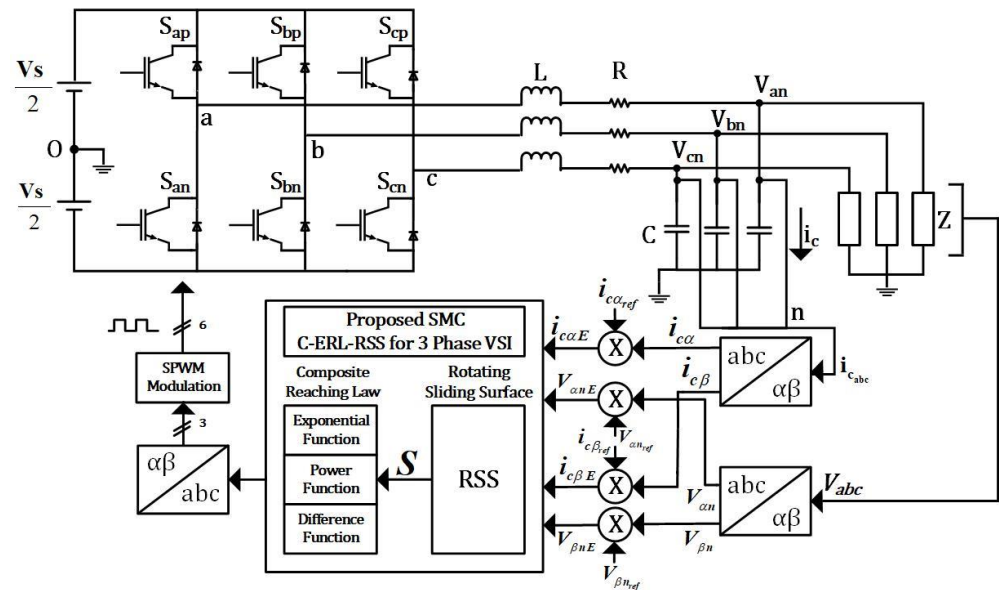


Figure 2. Three phase VSI with the proposed reaching law based SMC.

#### System Modeling for Three Phase VSI

Applying energy conservation laws (KVL/KCL) on the circuit shown in Figure 2, the following equalities can be deduced:

$$\begin{cases} Cv_{jn} = i_{cj} ; j = a, b, c \\ Lt_{Lj} + ri_{Lj} = u_{j0} - v_{jn} - v_{n0} ; v_{n0} = 0 \\ i_{Lj} = i_{cj} + \frac{v_{jn}}{Z_j} \\ v_{j0} = v_{jn} + v_{n0} \\ \sum_j i_{Lj} = \sum_j v_{jn} = 0 ; \text{Energy Conservation Law} \end{cases} \quad (1)$$

where each phase is represented by  $j = a, b, c$ . The capacitor voltage and current are represented by  $v_{jn}$  and  $i_{cj}$ , respectively. In order to decouple the  $abc$  axes,  $abc$  is transformed into a stationary  $\alpha\beta$  reference frame coordinate system. The following is the  $abc \sim \alpha\beta$  transformation matrix [27]:

$$T_{abc \sim \alpha\beta} = \frac{2}{3} \begin{bmatrix} 1 & -\frac{1}{2} & -\frac{1}{2} \\ 0 & -\frac{\sqrt{3}}{2} & \frac{\sqrt{3}}{2} \end{bmatrix} \quad (2)$$

The state space equation for three phase VSI with state variables  $v_{kn}$  and  $i_{Ck}$  in the stationary  $\alpha\beta$  reference frame can be derived as:

$$\begin{bmatrix} \dot{v}_{kn} \\ \dot{i}_{Ck} \end{bmatrix} = A \begin{bmatrix} v_{kn} \\ i_{Ck} \end{bmatrix} + Bu_k + D ; k = \alpha, \beta \quad (3)$$

where  $u_k$  represents the control input and after simplifying (1), matrices  $A$  and  $B$  are derived as:

$$A = \begin{bmatrix} 0 & \frac{1}{C} \\ -\frac{Z_j+r}{Z_jL} & -\left(\frac{1}{Z_jC} + \frac{r}{L}\right) \end{bmatrix} \text{ and } B = \begin{bmatrix} 0 \\ -\frac{V_s}{2L} \end{bmatrix}$$

Representing state variables  $\begin{bmatrix} v_{kn} \\ i_{Ck} \end{bmatrix}$  by  $x$ , (1) can be simplified as:

$$\dot{x} = Ax + Bu_k + D \quad (4)$$

The state space model of the system shown in (4) is the same for both axes, moreover, the following control design is valid to apply on any axes. In [30–32], a second order SMC with intelligent modifications was proposed for a three phase nonlinear system, so similarly, a second order SMC for a three phase VSI with a nonlinear load can be designed.

### 3. Sliding Mode Control Design

Following the characteristics of a three phase VSI, the capacitor current is the best reflection of change in the output voltage. Therefore, selecting the capacitor current error and voltage error as state variables leads to the best control design for output voltage regulation. The voltage error and capacitor current relation can be described as:

$$e = x_{ref} - x = \begin{bmatrix} e_1 \\ e_2 \end{bmatrix} \quad (5)$$

$$e_1 = v_{kref} - v_{kn} \quad (6)$$

$$e_2 = i_{Ckref} - i_{Ck} = \frac{1}{C} \dot{e}_1 \quad (7)$$

$$x_{aref} = \begin{bmatrix} v_{aref} \\ i_{Caref} \end{bmatrix} = \begin{bmatrix} V_o \sin(\omega t) \\ \omega V_o \cos(\omega t) \end{bmatrix} \quad (8)$$

$$x_{\beta ref} = \begin{bmatrix} v_{\beta ref} \\ i_{C\beta ref} \end{bmatrix} = \begin{bmatrix} V_o \sin(\omega t - 90^\circ) \\ \omega V_o \cos(\omega t - 90^\circ) \end{bmatrix} \quad (9)$$

where  $V_o$  is the amplitude of the required output voltage and  $\omega$  is the angular frequency. From (5)–(7), state space form (4) can be represented as:

$$\dot{e} = Ae + Bu_k + D \quad (10)$$

where  $D(t)$  is the disturbance term derived as a similar disturbance matrix  $D$  for the three phase VSI derived in [29]:

$$D(t) = \begin{bmatrix} 0 \\ C\ddot{v}_{kref} + \frac{\dot{v}_{kref}}{Z_k} + \frac{v_{kref}}{L} \end{bmatrix}$$

Generally, in SMC there are two modes of operations (i.e., the sliding mode and the reaching mode). In the reaching mode, the reaching law is applied to force the system state to reach the sliding surface quickly. Hence, an effective reaching law based on the distance of system states from the sliding surface ensures stability, which will be discussed later in the paper. Once the system states are on the sliding surface, the system is said to be in the sliding mode of operation. Moreover, during the sliding mode of operation,

robustness is guaranteed, and the dynamics of the three phase VSI can be determined through (4). An equivalent control law is applied to drive the system states along the sliding surface. Specific to the case of a three phase VSI, the switching frequency constraint leads to the zigzag movement of system states along the sliding surface, which eventually results in chattering. Aside from the stability and robustness achieved in the sliding mode and reaching phase, respectively, the steady state and dynamic performance of the system can only be achieved by catering to both the reaching law and sliding surface selection. Thus, both the reaching law and sliding surface simultaneously play their role to improve the performance of the SMC.

Therefore, in order to design a SMC for three phase VSIs, the following are the two most important parameters of interest:

#### *Appropriate Sliding Surface Selection*

Suitable sliding surface selection is one of the most vital concerns to address. Normally, the sliding surface is the linear function of state variables and can be represented as:

$$S = [\lambda \quad 1] \begin{bmatrix} e_1 \\ e_2 \end{bmatrix} = Ce \quad ; \quad \lambda > 0 \quad (11)$$

where  $\lambda$  is the coefficient of the sliding surface. The dynamic behavior of the sliding surface (11), in the absence of external disturbances on a surface, can be shown as:

$$S_\alpha = \lambda e_{1\alpha} + e_{2\alpha} = \lambda e_{1\alpha} + e_{1\alpha} = 0 \quad (12)$$

$$S_\beta = \lambda e_{1\beta} + e_{2\beta} = \lambda e_{1\beta} + e_{1\beta} = 0$$

In the phase plane  $(e_{1\alpha\beta} - e_{2\alpha\beta})$ ,  $S = 0$  represents a sliding line passing through the origin having slope of  $-\lambda$ .

$$e_{1\alpha\beta} = -\lambda e_{1\alpha\beta} \quad (13)$$

First order Equation (13) can be solved to express the output voltage error as:

$$e_{1\alpha\beta}(t) = e_{1\alpha\beta}(0)e^{-\lambda t} \quad ; \quad \lambda > 0 \quad (14)$$

Strictly positive real value of  $\lambda$  ensures asymptotic stability. With this, the significance of  $\lambda$  is well proven. Thus, the optimal value of  $\lambda$  can easily be determined, which depends upon the system state variables  $e_{1\alpha\beta}$  and  $e_{1\alpha\beta}$ . The SIFLC adopted by Komurkugil in [18] for a single phase VSI was modified with minor adjustments to make it viable to apply on three phase TLVSI. Therefore, the following linear function is used to rotate the surface with changing state space variables:

$$\lambda_\alpha^R(t) = -0.45E_{d\alpha}(t) + 0.5$$

$$\lambda_\beta^R(t) = -0.45E_{d\beta}(t) + 0.5$$

where  $\lambda_\alpha^R(t)$  and  $\lambda_\beta^R(t)$  are the rotating sliding coefficient for the  $\alpha$  and  $\beta$  stationary frame, respectively, and

$$E_{d\alpha}(t) = |E_{1\alpha}(t)| - |E_{2\alpha}(t)|; \quad E_{1\alpha}(t) = K_1 e_{1\alpha} \wedge E_{2\alpha} = K_2 e_{2\alpha}$$

$$E_{d\beta}(t) = |E_{1\beta}(t)| - |E_{2\beta}(t)|; \quad E_{1\beta}(t) = K_1 e_{1\beta} \wedge E_{2\beta} = K_2 e_{2\beta}$$

where  $K_1$  and  $K_2$  are the scaling gains. Following this, Equation (12) can be modified to the rotating sliding surface equation and can be represented as:

$$S_\alpha = \lambda_\alpha^R(t)e_{1\alpha} + e_{2\alpha} = 0$$



$$S_\beta = \lambda_\beta^R(t)e_{1\beta} + e_{2\beta} = 0$$

For simplicity, let us take  $S = S_{\alpha\beta}$  and from (6) and (7),  $e_1 = e_{1\alpha\beta}$ ,  $e_2 = e_{2\alpha\beta}$  and  $\lambda = \lambda_{\alpha\beta}^R$ ,

Thus (15) can be written as

$$S = \lambda_\beta^R(t)e_1 + e_2 = 0$$

### Proposed Composite Exponential Reaching Law for Three Phase VSI

In this section of the paper, mathematical formulation of the proposed composite exponential reaching law for the three phase VSI is presented. The proposed reaching law incorporates the benefits of the reaching laws referenced in the related work section and ensures an improved convergence rate than the traditional reaching laws. The proposed reaching law is an extension of the composite exponential reaching law proposed for a single phase VSI in [33].

**Stability Analysis:** The Lyapunov stability function is mentioned below, where  $S$  represents  $S_{\alpha\beta}$ :

$$\dot{V} = S^T \times \dot{S}$$

Hence, the stability condition  $\dot{V} < 0$  can be deduced as:

$$\begin{cases} \dot{S} < 0 & \text{if } S > 0 \\ \dot{S} > 0 & \text{if } S < 0 \end{cases}$$

The first derivative of (11) can be shown as:

$$\dot{S} = C\dot{e} \quad (15)$$

From (10) and (15), the control law can be represented as:

$$u_k = -\left(\dot{S} + CAe + CD\right)\left(CB^{-1}\right) \quad (16)$$

The reaching law is mathematically termed as the rate of change of the sliding surface. Therefore, the reachability principal and its significance in the control input can easily be visualized.

The proposed composite exponential reaching law (C-ERL) for a three phase VSI is given as:

$$\dot{S} = \left[ |S| \left( \mu + (1 - \mu)e^{-\gamma|S|^\delta} \right) - \frac{M|S|}{\mu + (1 - \mu)e^{-\gamma|S|^\delta} \cos(\varepsilon|S|)} \right] \text{sign}(S) \quad (17)$$

where  $0 < \mu < 1$ ,  $\gamma > 0$ ,  $\delta > 0$ ,  $M > 0$  and  $\varepsilon > 0$

The level of adaptability and effective nature of the proposed reaching law in (17) can be verified analytically under the following conditions:

- (i)  $S \gg 0$  : If the system states are far away from the sliding surface, a very high value of gain will be set to ensure the fast convergence of system states to the stable surface  $S = 0$ .
- (ii)  $S \approx 0$  : If the system states are close to the sliding surface,  $\mu + (1 - \mu)e^{-\gamma|S|^\delta} \cos(\varepsilon|S|) \approx 0$ , which leads to  $\frac{M|S|}{\mu + (1 - \mu)e^{-\gamma|S|^\delta} \cos(\varepsilon|S|)} < 1$  and  $|S| \left( \mu + (1 - \mu)e^{-\gamma|S|^\delta} \right) < \frac{M|S|}{\mu + (1 - \mu)e^{-\gamma|S|^\delta} \cos(\varepsilon|S|)}$ ; thus the value of overall gain set will be negligible and will mitigate chattering along the sliding surface.
- (iii)  $S \rightarrow 0$  : The values of  $\mu$ ,  $\gamma$ ,  $\delta$ , and  $\varepsilon$  are set in a way that the value of the reaching law gain becomes directly proportional to the distance of the system states from

the reference sliding surface  $S = 0$ . Assume that if  $e^{-\gamma|S|^\delta} \cos(\varepsilon|S|) \approx 0$ , then  $\mu + (1 - \mu)e^{-\gamma|S|^\delta} \cos(\varepsilon|S|) \approx \mu < 1$ , which eventually results in a higher value of  $\frac{M|S|}{\mu + (1 - \mu)e^{-\gamma|S|^\delta} \cos(\varepsilon|S|)}$ . Whereas  $|S| \left( \mu + (1 - \mu)e^{-\gamma|S|^\delta} \right) < \frac{M|S|}{\mu + (1 - \mu)e^{-\gamma|S|^\delta} \cos(\varepsilon|S|)}$ , the value of the reaching law gain is adjusted based on the distance of system states from  $S = 0$ .

Therefore, the value of reaching the law control gain set by the proposed reaching law for a three phase VSI adopts the most efficient convergence mechanism to force system states to the reference surface in finite time. From [20],  $e^{-\gamma|S|^\delta} \cos(\varepsilon|S|)$  was tailored with the proposed reaching law to achieve fast damping characteristics along the surface and force the system states to cross zero several times before reaching the origin and coincide asymptotically to the equilibrium surface. Furthermore,  $|S| \left( \mu + (1 - \mu)e^{-\gamma|S|^\delta} \right)$  in the reaching law serves to adjust and mitigate the gain value near the equilibrium surface to ensure extreme possible chattering reduction along the sliding surface.

Adaptability behavior for setting the reaching law control gain value with reference to the distance of system states from the equilibrium surface is shown in Figure 3, which shows a comparative analysis of the behavior of the state-of-the-art and latest reaching laws such as enhanced exponential reaching (EERL) [24], repetitive reaching law (RRL) [29], power rate exponential reaching law (PRERL) [27], and the proposed composite exponential reaching law with rotating sliding surface (C-ERL-RSS). The parametric values of the reaching law variables used in the analysis are mentioned in Table 1.

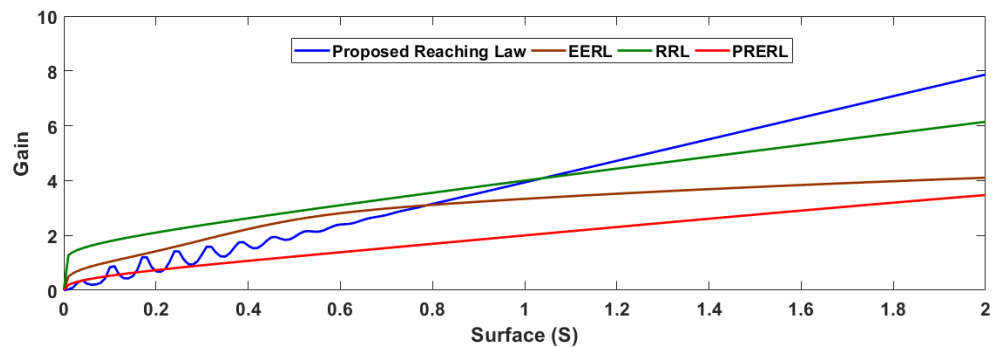


Figure 3. Reaching law gain adaptive behavior w.r.t distance of the surface from the equilibrium point.

Table 1. Parametric values of the reaching laws.

	Reaching Law	Parametric Values
EERL [24]	$\dot{S} = \left[ -KS - \frac{M S }{\mu + (1 - \mu)e^{-\gamma S ^\delta}} \right] \text{sign}(S)$	$\gamma = 10, \delta = 2, K = 10$ $\mu = 0.6, M = 2$
RRL [29]	$\dot{S} = [-KS - M S ^\tau] \text{sign}(S)$	$K = 10, M = 2, \tau = 0.3$
PRERL [27]	$\dot{S} = \left[ -\frac{M S ^\tau}{\mu + (1 - \mu)e^{-\gamma S ^\delta}} \right] \text{sign}(S)$	$\gamma = 10, \delta = 2, \tau = 0.3$ $\mu = 0.6, M = 2$
Proposed C-ERL-RSS	$\dot{S} = \left[  S  \left( \mu + (1 - \mu)e^{-\gamma S ^\delta} \right) - \frac{M S }{\mu + (1 - \mu)e^{-\gamma S ^\delta} \cos(\varepsilon S )} \right] \text{sign}(S)$	$\gamma = 10, \delta = 2, \varepsilon = 85$ [24] $\mu = 0.6, M = 2$

At distance  $S = 2$  far from the equilibrium point  $S = 0$ , the reaching law is supposed to set a higher value of gain to ensure a fast convergence rate to achieve a shorter reaching time. It is evident from Figure 3 that the proposed reaching law set the highest gain value at  $S = 2$  (i.e., gain = 8), thus, ensuring a fast convergence rate to achieve a shorter reaching time. Moreover, the reaching law must be capable of adjusting the gain value as the surface approaches the equilibrium point  $S = 0$ . The reaching law control gain value must be lowered



as the surface approaches  $S = 0$ ; following this condition, all reaching laws successfully fulfilled this criteria. The reaching law control gain value of the proposed C-ERL-RSS was lowered from RRL, EERL, and PRERL at  $S = 1.1$ ,  $S = 0.8$ , and  $S = 0.1$ , respectively.

However, very close to the equilibrium point  $S \approx 0$ , the reaching law control gain must diminish to overcome the curse of chattering along the sliding surface  $S = 0$ . It can be easily observed from Figure 2 that the value of the proposed C-ERL-RSS reaching law control gain was lowered compared to the other reaching law values, which almost vanished at  $S \approx 0$ . Therefore, it is obvious to conclude from the above discussion that the desired adoptive behavior for setting the reaching law control gain value is effectively fulfilled by the proposed C-ERL-RSS. The comparative analysis of the proposed C-ERL-RSS with the other reaching laws shown in Figure 3 is tabulated in Table 2.

**Table 2.** Reaching law behavior in terms of the reaching time and chattering.

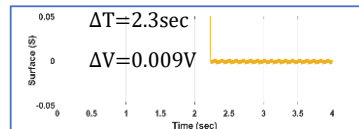
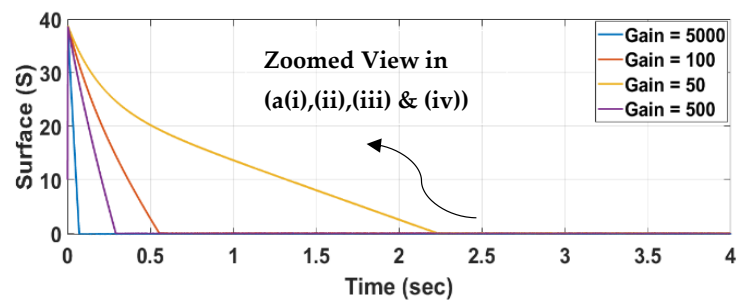
Reaching Law	Reaching Time	Chattering
EERL [24]	High	Moderate
RRL [29]	Moderate	High
PRERL [27]	High	Low
Proposed C-ERL-RSS	Low	Low

The proposed reaching law along with other state-of-the art reaching laws were implemented on the state space model of a three phase TLVSI in the stationary  $\alpha\beta$  reference frame shown in (4), and the comparative analysis of the performance of the proposed reaching law with other well-known reaching laws, on the basis of reaching time and chattering at different reaching law gain values, is presented in Figure 4a–d.

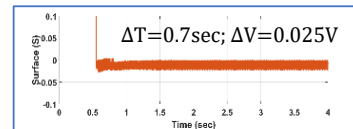
It is quite evident from Figure 4a,b that at a lower value of the reaching law gain (Gain = 50), the unwanted chattering along the sliding surface is negligible (i.e., 0.009 v and 0.1 v, respectively) while a reduction in chattering at such a low level is at the cost of a very high reaching time of 2.3 s and 2.2 s for PRERL and RRL, respectively. However, the problem of a high reaching time is handled better when applying higher gain values (i.e., reaching time at 100, 500, and 5000 are witnessed as 0.7 s, 0.3 s, and 0.2 s for PRERL and 0.45 s, 0.25 s and 0.18 s for RRL, respectively). The performance of the reaching law was measured based on the reduced reaching time and chattering simultaneously at different values of gain. Therefore, the chattering of PRERL at Gain = 100, Gain = 500, and Gain = 5000 was observed as 0.025 v, 0.035 v, and 0.45 v, respectively. Likewise, the chattering magnitude of RRL at Gain = 100, Gain = 500, and Gain = 5000 was measured as 0.015 v, 0.045 v, and 0.25 v, respectively. Therefore, performance of PRERL and RRL is a great compromise between the reaching time and chattering. As far as V2L application is concerned, a fast transient response with minimal chattering along the surface is necessary to derive critical loads.

Thus, the behavior of PRERL and RRL clearly shows that their performances were more or less similar in nature. One of the two desired benefits (i.e., reduced reaching time and mitigated chattering along the sliding surface) can be achieved at a specific value of gain, while a high reaching time, low chattering at higher values of gain, and low reaching time was obtained with a higher chattering magnitude. Moreover, if the adaptive nature of the reaching law is considered, this behavior of performance still leads to very low transient response as well as setting time. Therefore, the reaching law gain value cannot be mitigated to the desired level necessary to handle critical loads.

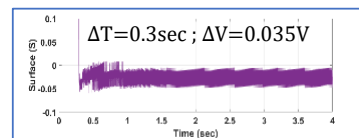
To some extent, the problem of high reaching time at a lower gain value of 50 was solved by EERL while maintaining a smaller chattering magnitude, as shown in Figure 4c. The reaching time was reduced to 1.7 s with a chattering of 0.015 v along the surface. Moreover, this improvement in behavior was also witnessed at higher values of gain (i.e., 100, 500, and 5000). The reaching time and chattering magnitude observed at 100, 500, and 5000 were 0.38 s, 0.3 s, 0.15 s, and 0.04 v, 0.05 v, 0.3 v, respectively.



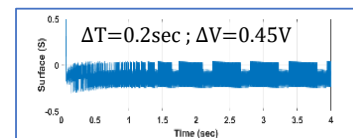
(i) Gain = 50



(ii) Gain = 100

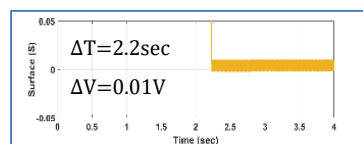
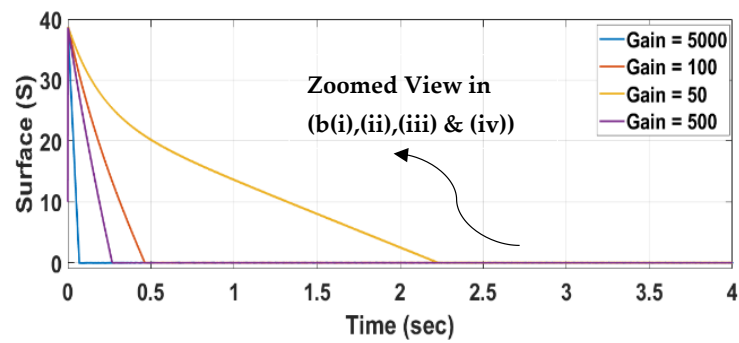


(iii) Gain = 500

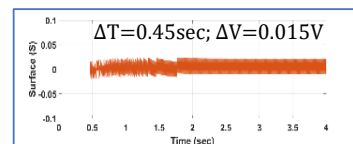


(iv) Gain = 5000

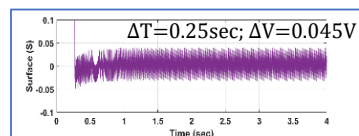
(a)



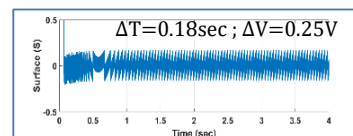
(i) Gain = 50



(ii) Gain = 100



(iii) Gain = 500



(iv) Gain = 5000

(b)

Figure 4. Cont.

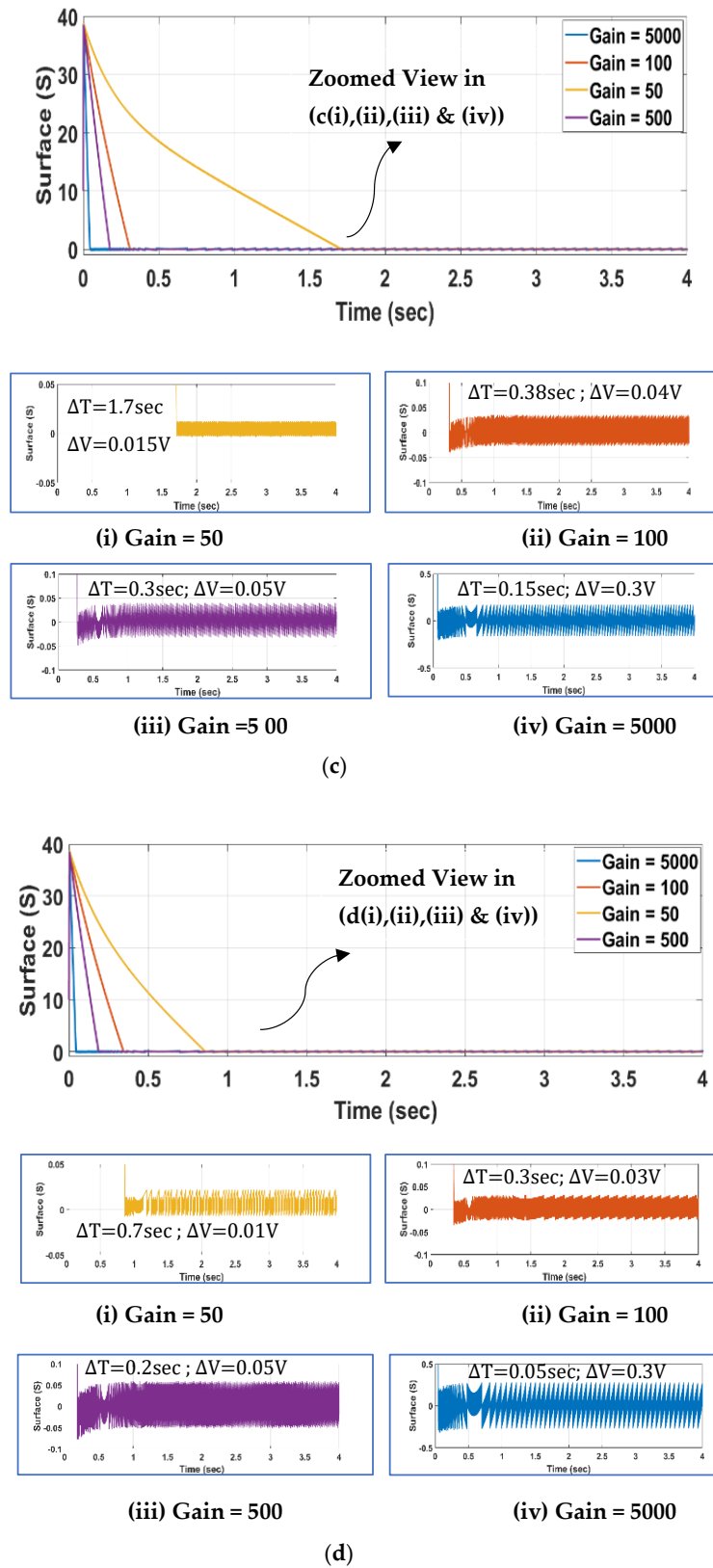


**Figure 4.** (a) PRERL-reaching law behavior at different gain values. Zoomed view to analyze the chattering and reaching time at 50, 100, 500, and 5000 gain values at (i), (ii), (iii), and (iv), respectively. (b) RRL-reaching law behavior at different gain values. Zoomed view to analyze the chattering and reaching time at 50, 100, 500 and 5000 gain values at (i), (ii), (iii), and (iv), respectively. (c) EERL-reaching

law behavior at different gain values. Zoomed view to analyze the chattering and reaching time at 50, 100, 500, and 5000 gain values at (i), (ii), (iii), and (iv), respectively. (d) Proposed C-ERL-RSS-reaching law for three phase VSI behavior at different gain values. Zoomed view to analyze the chattering and reaching time at 50, 100, 500 and 5000 gain values at (i), (ii), (iii), and (iv), respectively.

The performance of the proposed reaching law under different gain values is shown in Figure 4d. In order to achieve a reduced reaching time under a low value of gain (Gain = 50), the proposed reaching law has been proven to be the most effective among other reaching laws, while maintaining a low level of chattering along the sliding surface. The response shown in Figure 4d is further highlighted as the zoomed view in Figure 4d(i) for Gain = 50, and the reduced reaching time with minimal possible chattering level was found to be 0.7 s and 0.01 v. Moreover, this encouraging behavior was continuous even at higher values of gain (i.e., at Gain = 100), the reaching time was found to be 0.3 s with a chattering of 0.03 v along the surface, at Gain = 500 and Gain = 5000, the reaching time and chattering were observed as 0.2 s, 0.05 s and 0.05 V, 0.3 V, respectively.

It is worth mentioning here that at higher values of gain (i.e., 5000), the chattering magnitude of RRL, EERL, and proposed reaching law were very close to each other. Thus, the important factor to notice here is the outstanding reduction in reaching time of 0.05 s compared to the other reaching laws, while ensuring either very little or the same chattering level. Therefore, one can easily visualize the adaptive and effective nature of the proposed reaching law at different gain values to achieve a reduced reaching time with the minimum possible chattering level.

Following the behavior of the reaching laws shown in Figure 4, the relationship between chattering and reaching time at different values of gain is presented in Figure 5. A tremendous reduction in the reaching time at low value of gain (Gain = 50) was achieved through the proposed reaching law while maintaining a low level of chattering. Similarly, if we follow the trend down on the reaching time axis, the reaching time reduction behavior was highly reduced to 0.05 s while ensuring the minimum possible level of chattering. Likewise, in the case of Gain = 100 and Gain = 500, this reduction pattern of reaching time was also continuous with a slight increase in chattering. At Gain = 100, the reaching time was observed as 0.3 s with the chattering magnitude of 0.03 V, and at Gain = 500, the value of the reaching time was reduced to 0.02 s with 0.05 V of chattering magnitude along the sliding surface. While analyzing the behavior at the higher extreme value of gain (i.e., 5000), the reaching time was found to be extremely low at 0.03 s with a restricted chattering magnitude of 0.03 V. Concluding this, if a major concern of a sensitive system is that it switches performance at high frequencies (i.e., reduced chattering), the proposed reaching law at a lower value of gain solves the task by providing extremely low chattering while also ensuring a fast convergence time. On the other hand, PRERL [27], RRL [29], and EERL [24] offer a low magnitude of chattering but at the cost of a very high reaching time.

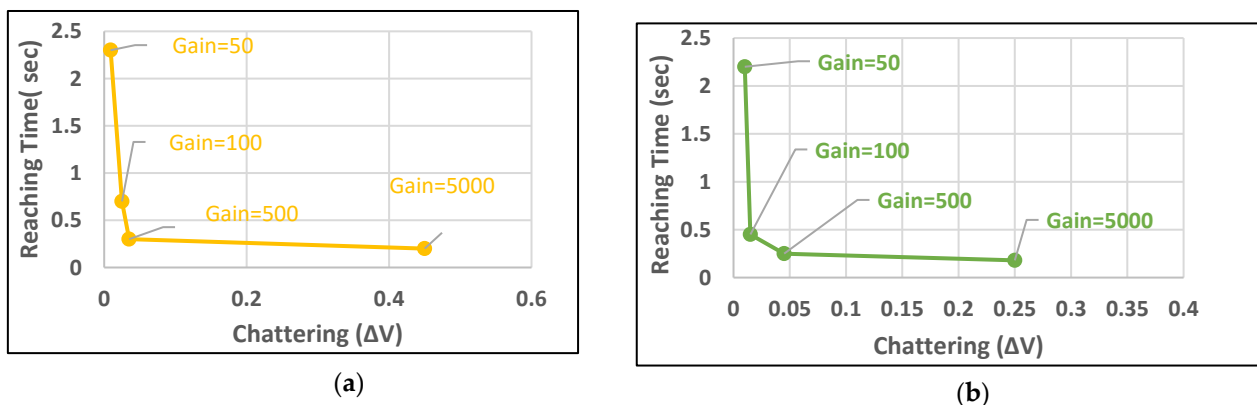
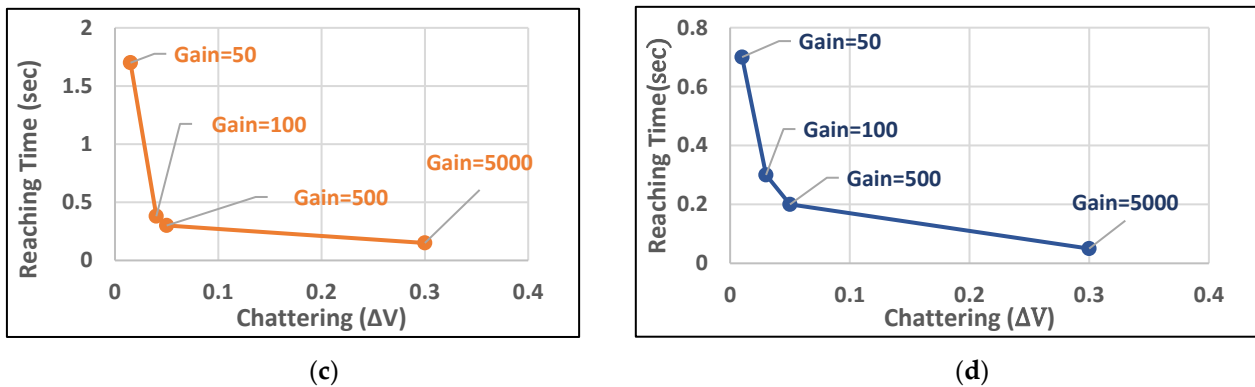


Figure 5. Cont.



**Figure 5.** Trade-off between reaching time and chattering on different gain values: (a) PRERL [27], (b) RRL [29], (c) EERL [24], (d) proposed C-ERL-RSS.

**4. SMC with Proposed Reaching Law**

Relation of the first derivative of the sliding surface, shown in (15), can also be represented as:

$$\dot{S} = \dot{e}_1\lambda + \dot{e}_2 = \dot{e}_1\lambda + \ddot{e}_1$$

Using (10),

$$\dot{S} = \dot{e}_1K - \frac{(r+Z)}{ZL}e_1 - \left(\frac{1}{ZC} + \frac{r}{L}\right)e_2 - \frac{V_s}{2L}u_k \tag{18}$$

Equating Equations (17) and (18),

$$\left[|S| \left(\mu + (1-\mu)e^{-\gamma|S|^\delta}\right) - \frac{M|S|}{\mu+(1-\mu)e^{-\gamma|S|^\delta} \cos(\epsilon|S|)}\right] \text{sign}(S) = \dot{e}_1\lambda - \frac{(r+Z)}{ZL}e_1 - \left(\frac{1}{ZC} + \frac{r}{L}\right)e_2 - \frac{V_s}{2L}u_k$$

$$u_k = -\frac{2L}{V_s} \left( \left[|S| \left(\mu + (1-\mu)e^{-\gamma|S|^\delta}\right) - \frac{M|S|}{\mu+(1-\mu)e^{-\gamma|S|^\delta} \cos(\epsilon|S|)}\right] \text{sign}(S) - \dot{e}_1\lambda + \frac{(r+Z)}{ZL}e_1 + \left(\frac{1}{ZC} + \frac{r}{L}\right)e_2 \right)$$

The control input for the  $\alpha\beta$  stationary frame can be segregated in (19) and (20),

$$u_\alpha = -\frac{2L}{V_s} \left( \left[|S| \left(\mu + (1-\mu)e^{-\gamma|S|^\delta}\right) - \frac{M|S|}{\mu+(1-\mu)e^{-\gamma|S|^\delta} \cos(\epsilon|S|)}\right] \text{sign}(S) - \dot{e}_{1\alpha}\lambda + \frac{(r+Z)}{ZL}e_{1\alpha} + \left(\frac{1}{ZC} + \frac{r}{L}\right)\frac{\dot{e}_{1\alpha}}{C} \right) \tag{19}$$

$$u_\beta = -\frac{2L}{V_s} \left( \left[|S| \left(\mu + (1-\mu)e^{-\gamma|S|^\delta}\right) - \frac{M|S|}{\mu+(1-\mu)e^{-\gamma|S|^\delta} \cos(\epsilon|S|)}\right] \text{sign}(S) - \dot{e}_{1\beta}\lambda + \frac{(r+Z)}{ZL}e_{1\beta} + \left(\frac{1}{ZC} + \frac{r}{L}\right)\frac{\dot{e}_{1\beta}}{C} \right) \tag{20}$$

*Simulation Study*

In this part of the article, the reference tracking trajectory of output voltage for RRL [29], PRERL [27], EERL [24], and the proposed reaching law is shown through the implementation of three phase TLVSI in MATLAB/Simulink. The performance of the aforementioned reaching laws along with the proposed reaching law was tested on three phase TLVSI under a nonlinear rectifier load of 1 KW with circuit parameters and specifications shown in Table 3. The diode bridge rectifier or DIAC/TRIAC controlled bridge rectifier is considered as a nonlinear load, and the behavior of the load current depends upon the type

of component (resistive/inductive) added at the output of a rectifier. In [19,34], a rectifier was used as a nonlinear load with a resistor at the output of the rectifier, which led to a sinusoidal output current waveform. However, in the case of [35], a rectifier was used as a nonlinear load with the inductor at the output, which leads to a distorted output current waveform. We used a diode bridge rectifier followed by a resistor as a nonlinear load to test our proposed SMC on a three phase VSI, which showed a sinusoidal shape of output current. Having said this, since the load is a rectifier, the load current witnesses zero crossover distortion. In our case, its value was very low, which one can observe as a zoomed view of the current wave form. Figure 6a,b shows the reference tracking trajectory of the output voltage and current response, respectively, from no load to full load condition at 0.025 s.

**Table 3.** Circuit specifications.

Circuit Parameters	Value
Input DC Voltage from Battery, $V_S$	500 V
Reference Voltage, $V_{RMS}$	220 V
Filter Inductor, $L$	4 mH
Filter Capacitor, $C$	30 $\mu$ F
Scaling Gain, $K_1$	$2 \times 10^{-3}$
Scaling Gain, $K_2$	$2.4 \times 10^{-5}$
Non-Linear Rectifier Load (Z)	1 KW
Switching Frequency, $f_s$ [14]	9 kHz
Fundamental Frequency $f$	50 Hz

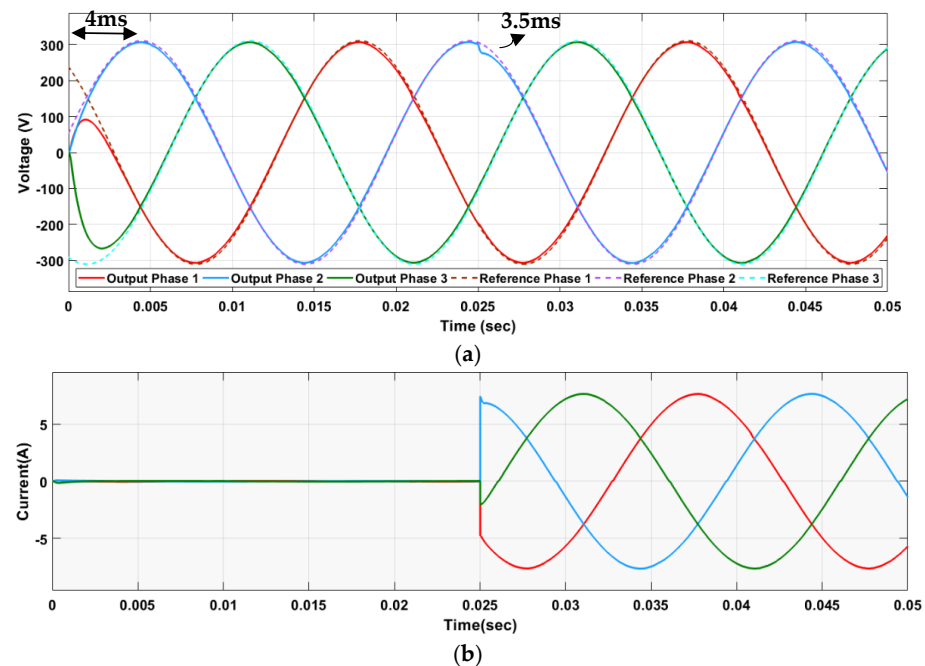


**Figure 6.** (a) PRERL [27], output voltage-reference tracking trajectory and voltage regulation. (b) PRERL [27], load current-step response under extreme load variation.

It is evident from Figure 6a that the output voltage started to track the reference voltage at 4 ms under no load condition. Moreover, there was a compromised voltage regulation beyond 4 ms. Similarly, the transient time was observed as 3.5 ms when the load was applied at 0.025 ms.

Likewise, the performance of the RRL [29] based SMC under aforementioned conditions is shown in Figure 7a,b. The reference tracking time under no load condition was not very encouraging as the output started at the following reference voltage at 7 ms with more compromised voltage regulation and comparatively slow transient response of 5 ms.



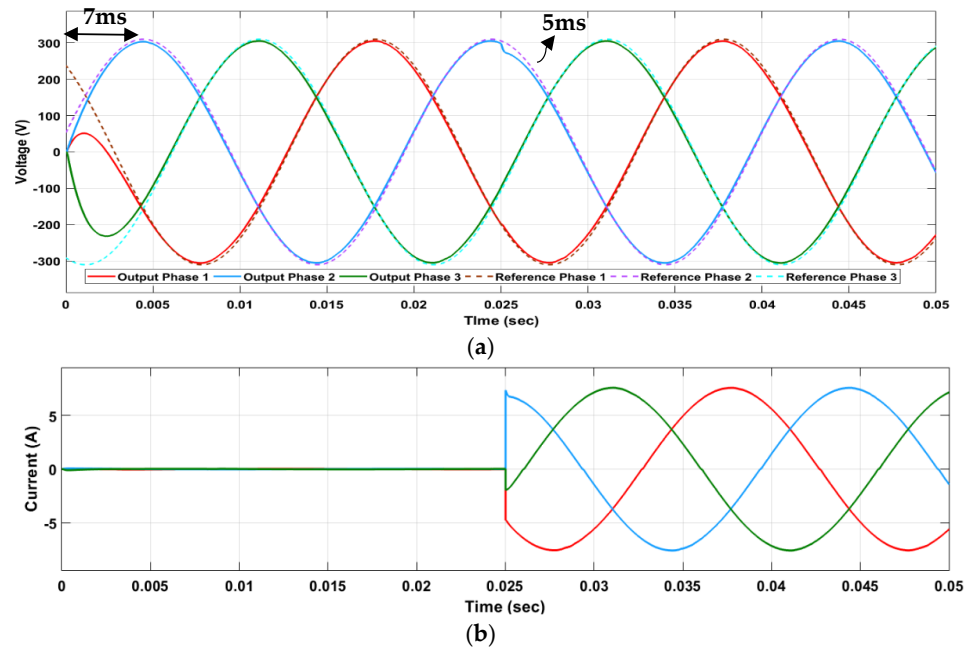


**Figure 7.** (a) RRL [29], output voltage-reference tracking trajectory and voltage regulation. (b) RRL [29], load current-step response under extreme load variation.

However, the response of EERL [24] based SMC, as shown in Figure 8a,b is quite encouraging in terms of the reduced reference tracking time under the no load condition as well as the fast transient response observed. In Figure 8a, the reference tracking and transient time were observed as 2.5 ms and 2 ms, respectively. Additionally, a better reference voltage tracking led to improved voltage regulation compared to RRL [29] and PRERL [27].

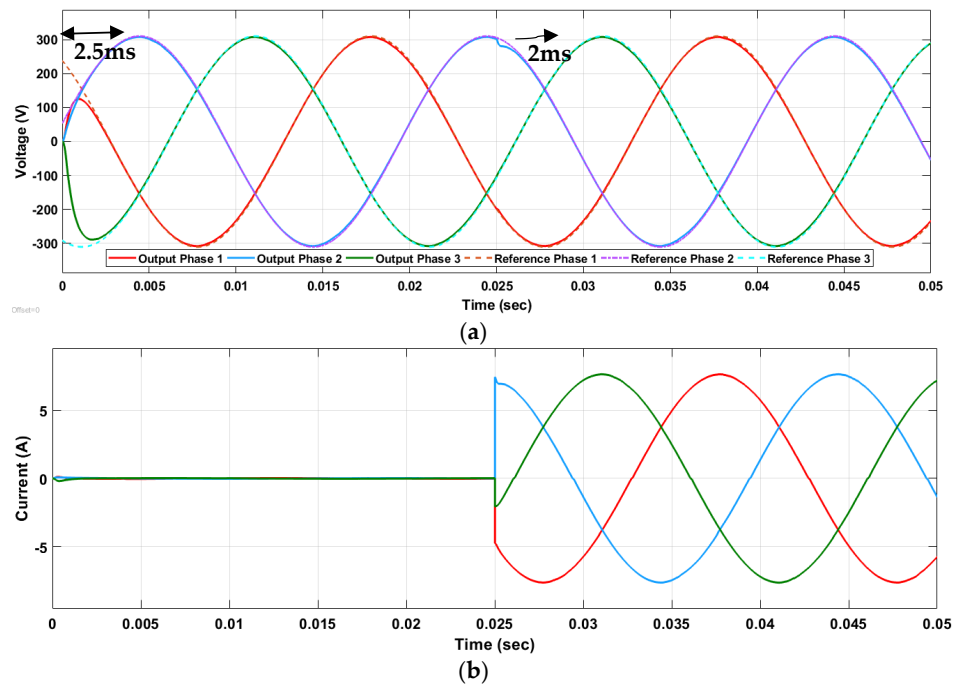


**Figure 8.** (a) EERL [24], output voltage-reference tracking trajectory and voltage regulation. (b) EERL [24], load current-step response under extreme load variation.

The performance of the proposed composite reaching law based SMC under predefined conditions for voltage regulation and trajectory tracking is shown in in Figure 9. An enormous reduction in reference tracking time of 0.08 ms was achieved with an extremely fast transient response of 0.05 ms at 0.025 s. A tremendous improvement in voltage regulation under no load and full load conditions was observed with an extremely low %THD of 1.1%.

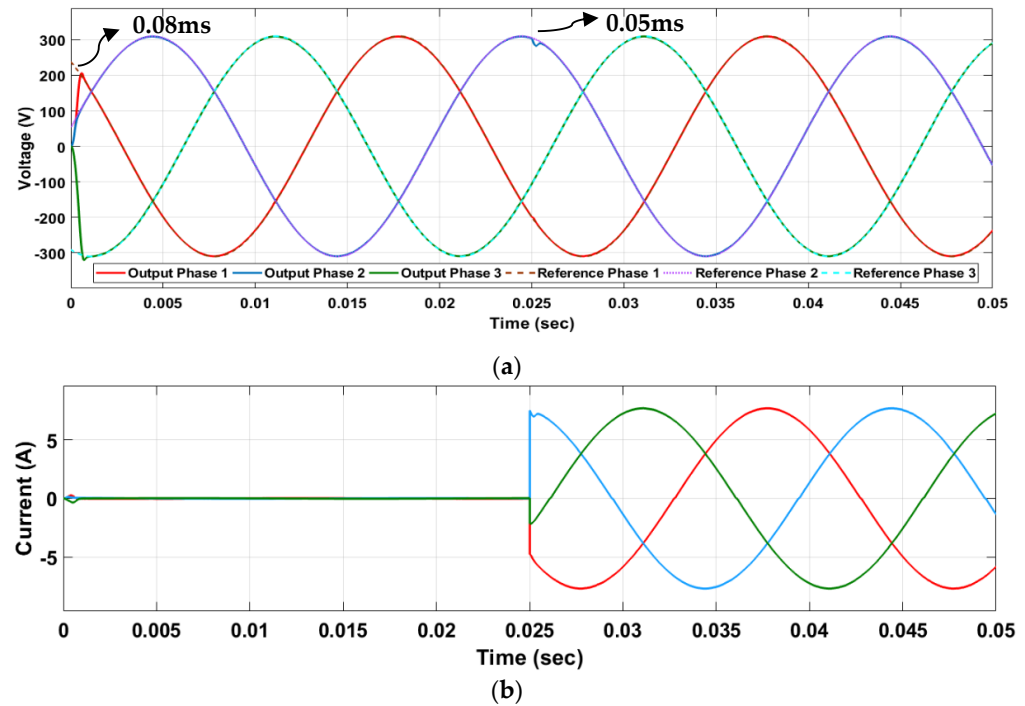


**Figure 9.** (a) Proposed C-ERL-RSS, output voltage-reference tracking trajectory and voltage regulation. (b) Proposed C-ERL-RSS, load current-step response under extreme load variations.

Therefore, the proposed reaching law based SMC has shown remarkable results to make it the most viable option to be used in EVs for V2L applications to handle critical loads.

A summary of the results of the comparative analysis obtained through the implementation of PRERL [27], RRL [29], EERL [24], and the proposed composite reaching law along with other state-of-the-art reaching laws based SMC results obtained from a similar system are shown in Table 4. It can be deduced from Table 4 that the proposed composite reaching law based SMC had extremely resilient behavior against sudden load variations. Moreover, a phenomenal reduction in %THD with a high level of voltage regulation makes the proposed composite reaching law the best among the other reaching laws.

**Table 4.** Comparison of the proposed composite reaching law with other state-of-the art reaching laws.

Controller	SMC [36]	DSMC [37]	TSMC [38]	PRERL [27] Compared in This Paper	RRL [29] Compared in This Paper	EERL [24] Compared in This Paper	Proposed C-ERL-RSS
Input— $V_{DC}$ (V)	360	250	250	500	500	500	500
Reference— $V_{RMS}$ (V)	220	110	110	220	220	220	220
Output— $V_{RMS}$ (V)	-	-	-	218	217	218.4	219.63
$f_{switching}$ (KHz)	15	10	20	09	09	09	09
%THD	1.7%	1.6%	5.1%	2.3%	3.2%	1.8%	1.1%
%Voltage Regulation	-	-	-	99.09%	98.63%	99.27%	99.83%
Robustness	-	-	-	Good	Good	Better	Best
Tracking Time (ms)	-	-	-	4	7	2.5	0.08
Transient Time (ms)	0.5	2	2	3.5	5	2	0.05

The event-driven tools are advantageous in terms of real-time compression and computing complexity reduction [39–41]. Future research can be conducted to access the feasibility of using these tools with the recommended methodology.

## 5. Experimental Results

As a proof of concept and to validate the competency and authenticity of the composite exponential reaching law, the proposed reaching law was implemented for single phase VSI through the smart integration of the Full Bridge Inverter Development Kit (SPM-FB-KIT) and DSP board (TMS320C6713 DSK) using the DC input voltage of  $V_s = 400$  V,  $V_{peak} = 300$  V, filter inductor  $L = 250$   $\mu$ H, and capacitor  $C = 100$   $\mu$ F, as depicted in Figure 10. Moreover, values of other scaling gains  $K_1$  and  $K_2$  were selected as  $2 \times 10^{-3}$  and  $2.4 \times 10^{-5}$ , respectively. Linear as well as nonlinear loads were selected to examine the experimental behavior of the proposed reaching law. In Figure 11a,b, the output voltage and current responses under linear and nonlinear load are shown, respectively. Figure 11a testifies to the capability of the proposed composite reaching law based SMC to achieve the required output voltage profile along with a stable load current and %THD of 0.69%. Moreover, the output voltage achieved under the nonlinear load condition shown in Figure 11b affirms the effectiveness of the proposed composite reaching law based SMC to achieve the required output voltage with a %THD of 1.12%.

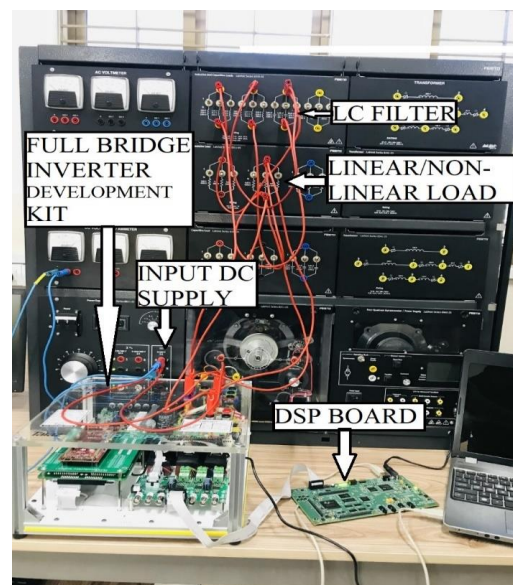


Figure 10. Experimental setup.

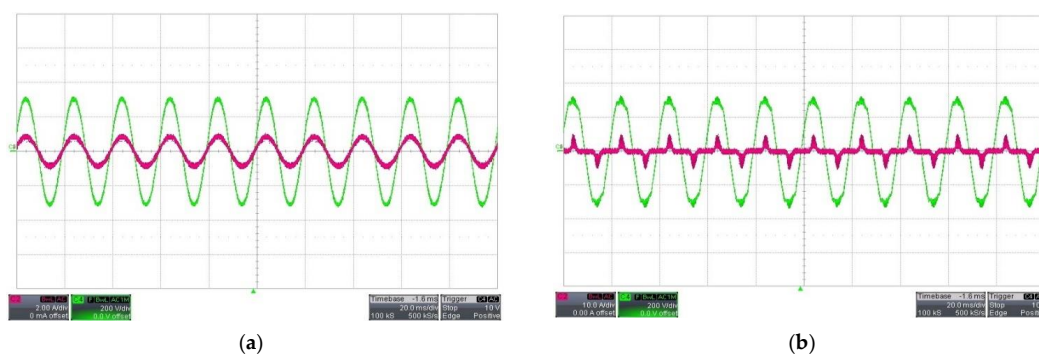


Figure 11. (a) Experimental output waveforms of voltage (green) 200 V/div and current (red) 2 A/div under a linear load. (b) Experimental output waveforms of voltage (green) 200 V/div and current (red) 10 A/div under a nonlinear load.

## 6. Conclusions

A novel composite reaching law based SMC was introduced for a three phase TLVSI to derive critical loads in V2L applications. The proposed composite reaching law based SMC made EVs more reliable in the V2L mode of operation to achieve a high level of robustness and fast convergence rate under variable load conditions. The comparative analysis advocates that the proposed composite reaching law has the wise mechanism of adjusting the gain values to achieve a fast convergence rate with reduced chattering, even at equilibrium point. The main concept of the proposed reaching law is to set the values of gain based on the distance of the state variable from the equilibrium surface (i.e., the gain value must be higher when state variables are far away from the equilibrium surface), similarly, the gain value must be reduced as the system state approaches the equilibrium point. Moreover, very close to the surface, the gain value must diminish to eliminate the chattering. Therefore, an intelligent mix of difference, power, and exponential functions was introduced to design the proposed composite reaching law. In addition, SIFLC was used for the selection of the optimal rotating sliding surface, the concept of which was based on a linear combination of system state variables. The performance of the proposed reaching law for three phase TLVSI verifies that the proposed reaching law offers a well-regulated output voltage with minimum %THD, better dynamic response and reduced chattering.

**Author Contributions:** Conceptualization, F.H., M.A., A.W. and S.M.Q.; methodology, F.H., M.A. and A.W.; implementation, F.H. and M.A.; validation, F.H., M.A., A.W. and S.M.Q.; formal analysis, F.H., M.A. and S.U.A.; investigation, F.H., M.A., A.W. and S.M.Q.; resources, A.W., S.M.Q. and A.T.A.; writing—original draft preparation, F.H., M.A. and A.W.; writing—review and editing, S.M.Q., S.U.A. and A.T.A.; visualization, F.H. and M.A.; supervision, M.A., A.W., S.M.Q. and A.T.A.; project administration, A.W., S.M.Q. and A.T.A.; funding acquisition, S.M.Q. and A.T.A. All authors have read and agreed to the published version of the manuscript.

**Funding:** The authors would like to thank the Effat University for funding this work under the research grant number (UC#9/2June2021/7.2-21(3)5).

**Institutional Review Board Statement:** Not applicable.

**Informed Consent Statement:** Not applicable.

**Data Availability Statement:** Not applicable.

**Acknowledgments:** The authors are grateful to Bahria School of Engineering and Applied Sciences, Bahria University Islamabad and Effat University, Jeddah, Saudi Arabia for technical support. The authors also acknowledge financial support from the Supply Chain Management Department of the Effat University and from the Electrical and Computer Engineering Department of the Effat University under the grant number (UC#9/2June2021/7.2-21(3)5), Effat University, Jeddah, Saudi Arabia.

**Conflicts of Interest:** The authors declare no conflict of interest.

## References

1. Barja-Martinez, S.; Rucker, F.; Aragues-Penalba, M.; Villafafila-Robles, R.; Munne-Collado, I.; Lloret-Gallego, P. A Novel Hybrid Home Energy Management System Considering Electricity Cost and Greenhouse Gas Emissions Minimization. *IEEE Trans. Ind. Appl.* **2021**, *57*, 2782–2790. [[CrossRef](#)]
2. Kanellos, F.D.; Grigoroudis, E.; Hope, C.; Kouikoglou, V.S.; Phillis, Y.A. Optimal GHG Emission Abatement and Aggregate Economic Damages of Global Warming. *IEEE Syst. J.* **2017**, *11*, 2784–2793. [[CrossRef](#)]
3. Houghton, J. *Global Warming the Complete Briefing*; Cambridge University Press: Cambridge, UK, 1994.
4. Yuan, J.; Dorn-Gomba, L.; Callegaro, A.D.; Reimers, J.; Emadi, A. A Review of Bidirectional On-Board Chargers for Electric Vehicles. *IEEE Access* **2021**, *9*, 51501–51518. [[CrossRef](#)]
5. Shirazul, I.; Iqbal, A.; Marzband, M.; Khan, I.; Al-Wahedi, A.M.A.B. State-of-the-art vehicle-to-everything mode of operation of electric vehicles and its future perspectives. *Renew. Sustain. Energy Rev.* **2022**, *166*, 112574.
6. Curkovic, M.; Jezernik, K.; Horvat, R. FPGA-Based Predictive Sliding Mode Controller of a Three-Phase Inverter. *IEEE Trans. Ind. Electron.* **2013**, *60*, 637–644. [[CrossRef](#)]
7. Sayed, K.; Almutairi, A.; Albagami, N.; Alrumayh, O.; Abo-Khalil, A.G.; Saleeb, H. A Review of DC-AC Converters for Electric Vehicle Applications. *Energies* **2022**, *15*, 1241. [[CrossRef](#)]

8. Hasan, M.; Mekhilef, S.; Ahmed, M. Three-phase hybrid multilevel inverter with less power electronic components using space vector modulation. *IET Power Electron.* **2014**, *7*, 1256–1265. [\[CrossRef\]](#)
9. Dezhi, X.; Liu, J.; Yan, X.; Yan, W. A novel adaptive neural network constrained control for a mul-ti-area interconnected power system with hybrid energy storage. *IEEE Trans. Ind. Electron.* **2017**, *65*, 6625–6634.
10. Chiang, S.; Tai, T.; Lee, T. Variable structure control of UPS inverters. *IEE Proc.-Electr. Power Appl.* **1998**, *145*, 559–567. [\[CrossRef\]](#)
11. Gudey, S.K.; Gupta, R. Recursive fast terminal sliding mode control in voltage source inverter for a low-voltage microgrid system. *IET Gener. Transm. Distrib.* **2016**, *10*, 1536–1543. [\[CrossRef\]](#)
12. Tai, T.-L.; Chen, J.-S. UPS inverter design using discrete-time sliding-mode control scheme. *IEEE Trans. Ind. Electron.* **2002**, *49*, 67–75. [\[CrossRef\]](#)
13. Iliev, B.; Hristozov, I. Variable structure control using Takagi-Sugeno fuzzy system as a sliding surface. In Proceedings of the 2002 IEEE International Conference on Fuzzy Systems, Honolulu, HI, USA, 12–17 May 2002; pp. 644–649.
14. Choi, S.-B.; Park, D.-W.; Jayasuriya, S. A time-varying sliding surface for fast and robust tracking control of second-order uncertain systems. *Automatica* **1994**, *30*, 899–904. [\[CrossRef\]](#)
15. Bartoszewicz, A. A comment on ‘A time-varying sliding surface for fast and robust tracking control of second-order uncertain systems’. *Automatica* **1995**, *31*, 1893–1895. [\[CrossRef\]](#)
16. Šabanovic, A. Variable structure systems with sliding modes in motion control—A survey. *IEEE Trans. Ind. Informat.* **2011**, *7*, 212–223. [\[CrossRef\]](#)
17. Tokat, S.; Eksin, I.; Guzelkaya, M. New approaches for on-line tuning of the linear sliding surface slope in sliding mode controllers. *Turkish J. Elect. Eng.* **2003**, *11*, 45–59.
18. Yorgancioglu, F.; Kömürçügil, H. Single-input fuzzy-like moving sliding surface approach to the sliding mode control. *Electr. Eng.* **2008**, *90*, 199–207. [\[CrossRef\]](#)
19. Komurcugil, H. Rotating-Sliding-Line-Based Sliding-Mode Control for Single-Phase UPS Inverters. *IEEE Trans. Ind. Electron.* **2012**, *59*, 3719–3726. [\[CrossRef\]](#)
20. Brahmi, B.; Laraki, M.H.; Brahmi, A.; Saad, M.; Rahman, M.H. Improvement of sliding mode controller by using a new adaptive reaching law: Theory and experiment. *ISA Trans.* **2020**, *97*, 261–268. [\[CrossRef\]](#)
21. Wu, L.; Liu, J.; Vazquez, S.; Mazumder, S.K. Sliding Mode Control in Power Converters and Drives: A Review. *IEEE/CAA J. Autom. Sin.* **2022**, *9*, 392–406. [\[CrossRef\]](#)
22. Gao, W.; Hung, J.C. Variable structure control of nonlinear systems: A new approach. *IEEE Trans. Ind. Electron.* **1993**, *40*, 45–55. [\[CrossRef\]](#)
23. Huang, J.; Zhang, Z.; Han, J.; Jiang, W. Sliding mode control of permanent magnet generator sys-tem based on improved exponential rate reaching law. *IET Electr. Power Appl.* **2020**, *14*, 154–1162. [\[CrossRef\]](#)
24. Mozayan, S.M.; Saad, M.; Vahedi, H.; Fortin-Blanchette, H.; Soltani, M. Sliding Mode Control of PMSG Wind Turbine Based on Enhanced Exponential Reaching Law. *IEEE Trans. Ind. Electron.* **2016**, *63*, 6148–6159. [\[CrossRef\]](#)
25. Liu, Y.; Wang, Z.; Xiong, L.; Wang, J.; Jiang, X.; Bai, G.; Li, R.; Liu, S. DFIG wind turbine sliding mode control with exponential reaching law under variable wind speed. *Int. J. Electr. Power Energy Syst.* **2018**, *96*, 253–260. [\[CrossRef\]](#)
26. Fallaha, C.J.; Saad, M.; Kanaan, H.Y.; Al-Haddad, K. Sliding-Mode Robot Control With Exponential Reaching Law. *IEEE Trans. Ind. Electron.* **2011**, *58*, 600–610. [\[CrossRef\]](#)
27. Devika, K.B.; Thomas, S. Power rate exponential reaching law for enhanced performance of sliding mode control. *Int. J. Control Autom. Syst.* **2017**, *15*, 2636–2645. [\[CrossRef\]](#)
28. Rohith, G. Fractional power rate reaching law for augmented sliding mode performance. *J. Frankl. Inst.* **2021**, *358*, 856–876. [\[CrossRef\]](#)
29. Zheng, L.; Jiang, F.; Song, J.; Gao, Y.; Tian, M. A Discrete-Time Repetitive Sliding Mode Control for Voltage Source Inverters. *IEEE J. Emerg. Sel. Top. Power Electron.* **2017**, *6*, 1553–1566. [\[CrossRef\]](#)
30. Liu, J.; Shen, X.; Alcaide, A.M.; Yin, Y.; Leon, J.I.; Vazquez, S.; Wu, L.; Franquelo, L.G. Sliding Mode Control of Grid-Connected Neutral-Point-Clamped Converters Via High-Gain Observer. *IEEE Trans. Ind. Electron.* **2021**, *69*, 4010–4021. [\[CrossRef\]](#)
31. Yunfei, Y.; Liu, J.; Sanchez, J.A.; Wu, L.; Vazquez, S.; Leon, J.I.; Franquelo, L.G. Observer-based adaptive sliding mode control of NPC converters: An RBF neural network approach. *IEEE Trans. Power Electron.* **2018**, *34*, 3831–3841.
32. Shen, X.; Liu, J.; Alcaide, A.M.; Yin, Y.; Leon, J.I.; Vazquez, S.; Wu, L.; Franquelo, L.G. Adaptive Second-Order Sliding Mode Control for Grid-Connected NPC Converters With Enhanced Disturbance Rejection. *IEEE Trans. Power Electron.* **2021**, *37*, 206–220. [\[CrossRef\]](#)
33. Haroon, F.; Aamir, M.; Waqar, A. Second-Order Rotating Sliding Mode Control with Composite Reaching Law for Two Level Single Phase Voltage Source Inverters. *IEEE Access* **2022**, *10*, 60177–60188. [\[CrossRef\]](#)
34. Cortes, P.; Ortiz, G.; Yuz, J.I.; Rodriguez, J.; Vazquez, S.; Franquelo, L.G. Model Predictive Control of an Inverter with Output LC Filter for UPS Applications. *IEEE Trans. Ind. Electron.* **2009**, *56*, 1875–1883. [\[CrossRef\]](#)
35. Rahmani, S.; Mendalek, N.; Al-Haddad, K. Experimental Design of a Nonlinear Control Technique for Three-Phase Shunt Active Power Filter. *IEEE Trans. Ind. Electron.* **2010**, *57*, 3364–3375. [\[CrossRef\]](#)
36. Merabet, A.; Labib, L.; Ghias, A.M.Y.M.; Ghenai, C.; Salameh, T. Robust Feedback Linearizing Control with Sliding Mode Compensation for a Grid-Connected Photovoltaic Inverter System Under Unbalanced Grid Voltages. *IEEE J. Photovolt.* **2017**, *7*, 828–838. [\[CrossRef\]](#)



37. Lopez-Santos, O.; Martinez-Salamero, L.; Garcia, G.; Valderrama-Blavi, H.; Sierra-Polanco, T. Robust Sliding-Mode Control Design for a Voltage Regulated Quadratic Boost Converter. *IEEE Trans. Power Electron.* **2015**, *30*, 2313–2327. [[CrossRef](#)]
38. Chang, F.-J.; Chang, E.-C.; Liang, T.-J.; Chen, J.-F. Digital-signal-processor-based DC/AC inverter with integral-compensation terminal sliding-mode control. *IET Power Electron.* **2011**, *4*, 159–167. [[CrossRef](#)]
39. Mian Qaisar, S. Event-Driven Coulomb Counting for Effective Online Approximation of Li-ion Battery State of Charge. *Energies* **2020**, *13*, 5600. [[CrossRef](#)]
40. Qaisar, S.M.; Khan, S.I.; Dallet, D.; Tadeusiewicz, R.; Pławiak, P. Signal-piloted processing metaheuristic optimization and wavelet decomposition based elucidation of arrhythmia for mobile healthcare. *Biocybern. Biomed. Eng.* **2022**, *42*, 681–694. [[CrossRef](#)]
41. Qaisar, S.M.; Alsharif, F. Signal Piloted Processing of the Smart Meter Data for Effective Appliances Recognition. *J. Electr. Eng. Technol.* **2020**, *15*, 2279–2285. [[CrossRef](#)]

**Disclaimer/Publisher’s Note:** The statements, opinions and data contained in all publications are solely those of the individual author(s) and contributor(s) and not of MDPI and/or the editor(s). MDPI and/or the editor(s) disclaim responsibility for any injury to people or property resulting from any ideas, methods, instructions or products referred to in the content.